Inorg. Chem. **2006**, *45*, 8120–8125

Two Mixed-Valence Vanadium(III,IV) Phosphonoacetates with 16-Ring Channels: $H_2(DABCO)[V^{IV}O(H_2O)V^{III}(OH)(O_3PCH_2CO_2)_2]\cdot 2.5H_2O$ and $H_2(PIP)[V^{IV}O(H_2O)V^{III}(OH)(O_3PCH_2CO_2)_2]\cdot 2.5H_2O$

Xian-Ming Zhang,* Juan-Juan Hou,[†] Wei-Xiong Zhang,[‡] and Xiao-Ming Chen[‡]

School of Chemistry & Material Science, Shanxi Normal University, Linfen, Shanxi 041004, China, and School of Chemistry and Chemical Engineering, Sun Yat-Sen University, Guangzhou 510275, P. R. China

Received May 6, 2006

Two isostructural mixed-valence vanadium phosphonoacetates $H_2(DABCO)[V^{IV}O(H_2O)V^{III}(OH)(O_3PCH_2CO_2)_2]\cdot 2.5H_2O$ (**1**) and $H_2(PIP)[V^{IV}O(H_2O)V^{III}(OH)(O_3PCH_2CO_2)_2]\cdot 2.5H_2O$ (**2**) have been synthesized. They crystallize in the orthorhombic space group *Pnna* with $a = 7.0479(10)$ Å, $b = 15.307(2)$ Å, and $c = 17.537(3)$ Å for **1** and $a = 7.0465(9)$ Å, $b = 15.646(2)$ Å, and $c = 17.396(2)$ Å for **2**. X-ray single-crystal diffraction reveals that **1** and **2** have a three-dimensional open framework featuring 16-ring ellipsoid channels that are filled with doubly protonated 1,4-diazabicyclo[2,2,2]octanium/piperazinium cations and water molecules. According to the classification in metal–organic frameworks, **1** and **2** contain infinite $(-O-V-)_\infty$ chains that are cross-linked by "metalloligand" $[VO(H_2O)(O_3PCH_2CO_2)_2]^{4-}$ into a 3-D net of the **sra** topology. The temperature dependence of the magnetic susceptibility of **1** shows that the $\chi_m T$ value in the range of 60–320 K is constant of 1.105 cm^3 K mol^{-1}/V_2 unit, and upon further cooling, the $\chi_m T$ value rapidly increases to 1.81 cm^3 K mol^{-1} at 2 K. The corresponding effective magnetic moment $(\mu_{eff})/V_2$ unit varies from 2.97 μ_B at 320 K to 3.80 μ_B at 2 K. The magnetic data in the range of 2–320 K follow the Curie–Weiss law with $C = 1.074$ cm^3 K mol^{-1} and $\Theta = -1.34$ K.

Introduction

Crystalline porous inorganic materials represented by aluminosilicates and metal phosphates are important in material science and industry.[1−5] Recently, several breakthroughs in the world of crystalline porous materials have been achieved by the use of metal−organic frameworks that are composed of metal centers or polynuclear clusters and organic linkers.[6] Metal organophosphonate open framework materials, which are structurally located between zeolite-like materials and metal−organic framework materials, have attracted recent attention due to their use in catalysis, separation, and ion-exchange and their potential future use as hybrid composite materials in electronic, optical, and sensing applications.[7] When transition metal ions such as V, Cr, Mn, Fe, Co, Ni, and Cu are included, which can be paramagnetic, metal organophosphonates can provide interesting examples of magnetic materials.[8] Phosphonic acid ligands, H_2O_3P-R-Z, are flexible, because they can be

* To whom correspondence should be addressed. E-mail: zhangxm@dns.sxnu.edu.cn. Fax and tel: int. code +86 357 2051402.
[†] Shanxi Normal University.
[‡] Sun Yat-Sen University.

(1) Breck, D. W. *Zeolite Molecular Sieves*; Kreiger: Malabar, FL, 1974.
(2) Barrer, R. M. *Hydrothermal Chemistry of Zeolites*; Academic Press: London, 1982.
(3) Szostak, R. *Molecular Sieves-Principles of Synthesis and Identification*, 2nd ed.; Blackie: London, 1998.
(4) Cheetham, A. K.; Ferey, G.; Loiseau, T. *Angew. Chem., Int. Ed.* **1999**, *38*, 3268.
(5) Cundy, S.; Cox, P. A. *Chem. Rev.* **2003**, *103*, 663.
(6) For recent reviews, see the following: (a) Kitagawa, S.; Kitaura, R.; Noro, S. *Angew. Chem., Int. Ed.* **2004**, *43*, 2334. (b) Rao, C. N. R.; Natarajan, S.; Vaidhyanathan, R. *Angew. Chem., Int. Ed.* **2004**, *43*, 1466. (c) Bradshaw, D.; Claridge, J. B.; Cussen, E. J.; Prior, T. J.; Rosseinsky, M. J. *Acc. Chem. Res.* **2005**, *38*, 273. (d) Ferey, G.; Mellot-Draznieks, C.; Serre, C.; Millange, F. *Acc. Chem. Res.* **2005**, *38*, 217. (e) Ockwig, N. W.; Delgado-Friedrichs, O.; O'Keeffe, M.; Yaghi, O. M. *Acc. Chem. Res.* **2005**, *38*, 176. (f) Suslick, K. S.; Bhyrappa, P.; Chou, J.-H.; Kosal, M. E.; Nakagaki, S.; Smithenry, D. W.; Wilson, S. R. *Acc. Chem. Res.* **2005**, *38*, 283. (g) Papaefstathiou, G. S.; MacGillivray, L. R. *Coord. Chem. Rev.* **2003**, *246*, 169. (i) Evans, O. R.; Lin, W. *Acc. Chem. Res.* **2002**, *35*, 511.
(7) For reviews, see the following: (a) Maeda, K. *Microporous Mesoporous Mater.* **2004**, *73*, 47. (b) Clearfield, A. *Chem. Mater.* **1998**, *10*, 2801. (c) Clearfield, A. In *Progress in Inorganic Chemistry*; Karlin, K. D., Ed.; John Wiley and Sons: New York, 1998; Vol. 47, pp 371−510. (d) Hix, G. B.; Turner, A.; Kariuki, B. M.; Tremayne, M.; MacLean, E. J. *J. Mater. Chem.* **2002**, *12*, 3220.
(8) Bellitto, C. In *Magnetism: Molecules to Materials*; Miller, J. S., Drillon, M.; Eds.; Wiley-VCH: Weinheim, Germany, 2001; Vol. 2, p 425.

10.1021/ic060771p CCC: $33.50
Published on Web 09/07/2006

functionalized by Z functional groups such as $-NH_2$, $-CO_2H$, $-SH$, and $-PO_3H_2$.[9−29] The structures of metal phosphonates can be directly influenced by Z functional ends, R groups, and metal ions. For M(IV) phosphonates, the structures can typically be described as an inorganic layer, consisting of M(IV) ions octahedrally coordinated by PO_3 groups, with the organic functional group pendant in the interlayer region.[30−32] For M(II) and M(III) phosphonates, structures are diverse in nature and often depend on the nature of the organic group and the metal being used.[7a] Before 1995, the majority of the M(II) and M(III) phosphonates reported were lamellar with the phosphonate anion pendant in the interlayer region. After 1995, the M(II) and M(III) phosphonates often contain metal atoms in nonoctahedral coordination environments and the organic phosphonate chains with Z functional groups that act as Lewis bases and coordinate to the metal ions in addition to the PO_3 groups. The cross-linking of metal ions by Z functional groups and PO_3 groups sometimes results in the formation of porous materials.

Although notable progress has been made in the construction of microporous metal organophosphonates, less progress has been achieved in the synthesis of organically templated mixed-valence transition metal organophosphonates.[7] Only several mixed-valence transition metal organophosphonates such as $Cs[(VO)_2V(O_3P(CH_2)PO_3)_2(H_2O)_2]$ and $Cu^{I}_2Cu^{II}(hedpH_2)_2(4,4'\text{-bpy})_2\cdot 2H_2O$ have been documented.[29] Generally, mixed-valence transition metal organophosphonates are more interesting than single-valence metal organophosphonates because they possibly will show redox catalysis and unusual magnetic behavior. In addition, single crystals of metal phosphonates suitable for X-ray structural analysis often are difficult to obtain from traditional methods (direct reaction of phosphonic acid with metal source by hydrothermal method, by refluxing, or by making metal salts contact with molten phosphonic acid) due to rapid crystallization.[33] An alternative way to achieve single crystals of metal phosphonates is to replace traditional routes by in situ hydrothermal hydrolysis of alkyl phosphonate route.[33−37] Often, this route turns out to be the only method to obtain single crystals of metal phosphonates. In this paper, we present two novel three-dimensional (3-D) organic templated mixed-valence vanadium(III/IV) phosphonoacetates featuring 16-ring channels, $H_2(DABCO)[V^{IV}O(H_2O)V^{III}(OH)(O_3PCH_2CO_2)_2]\cdot 2.5H_2O$ (**1**) and $H_2(PIP)[V^{IV}O(H_2O)V^{III}(OH)(O_3PCH_2CO_2)_2]\cdot 2.5H_2O$ (**2**) (DABCO = 1,4-diazabicyclo[2,2,2]-octane, PIP = piperazine, H_2DABCO = diprotonated DABCO, H_2PIP = diprotonated piperazine). In contrast to other micoporous metal phosphonocarboxylates, compounds **1** and **2** contain infinite $(-O-V-)_\infty$ chains that are cross linked by "metalloligand" $[VO(H_2O)(O_3PCH_2CO_2)_2]^{4-}$ into 3-D net of **sra** topology.[38]

Experimental Section

Materials and Methods. All the starting materials were purchased commercially reagent grade and used without further purification. Elemental analyses were performed on a Perkin-Elmer 240 elemental analyzer. The FT-IR spectra were recorded from KBr pellets in the range 500−4000 cm^{-1} on a Perkin-Elmer SPECTRUM BXII spectrometer. Thermal gravimetric analyses were performed under static air atmosphere using a Perkin-Elmer 7 thermogravimetric analyzer with a heating rate of 10 °C min^{-1}. XRPD data were recorded in a Bruker D8 ADVANCE X-ray powder diffractometer (Cu Kα, λ = 1.5418 Å). The magnetic measurements were carried out with Quantum Design SQUID MPMS XL-7 instruments. The diamagnetism of the sample and sample holder were taken into account.

Synthesis. $H_2(DABCO)[V^{IV}O(H_2O)V^{III}(OH)(O_3PCH_2CO_2)_2]\cdot 2.5H_2O$ (1). A mixture of $VOSO_4$ (0.147 g, 0.9 mmol), triethyl phosphonoacetate (0.146 g, 0.64 mmol, purchased from ACROS), 1,4-diazabicyclo[2,2,2]octane (DABCO) (0.70 g, 0.31 mmol), and H_2O (6 mL) in the molar ratio of 3:2:1:1100 was stirred in air, to which two drops of hydrofluoric acid (35%) was added to pH ≈ 4. The resulting solution was transferred into 15 mL Teflon-lined stainless steel reactor, which was heated at 170 °C for 120 h. After cooling of the sample to room temperature, blue-green crystals of **1** (65%) in a single phase were recovered. The measured pH value

(9) Neff, G. A.; Helfrich, M. R.; Clifton, M. C.; Page, C. J. *Chem. Mater.* **2000**, *12*, 2363.
(10) Guliants, V. V.; Benziger, J. B.; Sundaresan, S. *Chem. Mater.* **1995**, *7*, 1493.
(11) Kijima, T.; Watanabe, S.; Machida, M. *Inorg. Chem.* **1994**, *33*, 2586.
(12) Zheng, L.-M.; Duan, C.-Y.; Ye, X.-R.; Zhang, L.-Y.; Wang, C.; Xin, X.-Q. *J. Chem. Soc., Dalton Trans.* **1998**, 905.
(13) Rabu, P.; Janvier, P.; Bujoli, B. *J. Mater. Chem.* **1999**, *9*, 1323.
(14) Serpaggi, F.; Ferey, G. *Inorg. Chem.* **1999**, *38*, 4741.
(15) Ayyappan, S.; Delgado, G. D.; Cheetham, A. K.; Ferey, G.; Rao, C. N. R. *J. Chem. Soc., Dalton Trans.* **1999**, 2905.
(16) Ngo, H. L.; Lin, W. B. *J. Am. Chem. Soc.* **2002**, *124*, 14298.
(17) Midollini, S.; Orlandini, A.; Rosa, P.; Sorace, L. *Inorg. Chem.* **2005**, *44*, 2060.
(18) Fanucci, G. E.; Krzystek, J.; Meisel, M. W.; Brunel, L.-C.; Talham, D. R. *J. Am. Chem. Soc.* **1998**, *120*, 5469.
(19) Amicangelo, J. C.; Rosenthal, G. L.; Leenstra, W. R. *Chem. Mater.* **2003**, *15*, 390.
(20) Khan, M. I.; Lee, Y.-S.; O'Connor, C. J.; Haushalter, R. C.; Zubieta, J. *Chem. Mater.* **1994**, *6*, 721.
(21) Doran, M. B.; Norquist, A. J.; O'Hare, D. *Chem. Mater.* **2003**, *15*, 1449.
(22) Lohse, D. L.; Sevov, S. C. *Angew. Chem., Int. Ed. Engl.* **1997**, *36*, 1619.
(23) Khan, M. I.; Lee, Y.-S.; O'Connor, C. J.; Haushalter, R. C.; Zubieta, J. *J. Am. Chem. Soc.* **1994**, *116*, 4525.
(24) Zhu, J.; Bu, X.; Feng, P.; Stucky, G. D. *J. Am. Chem. Soc.* **2000**, *122*, 11563.
(25) Distler, A.; Sevov, S. C. *Chem. Commun.* **1998**, 959.
(26) Jankovics, H.; Daskalakis, M.; Raptopoulou, C. P.; Terzis, A.; Tangoulis, V.; Giapintzakis, J.; Kiss, T.; Salifoglou, A. *Inorg. Chem.* **2002**, *41*, 3366.
(27) Hartman, S. J.; Todorov, E.; Cruz, C.; Sevov, S. C. *Chem. Commun.* **2000**, 1213.
(28) Bauer, E. M.; Bellitto, C.; Colapietro, M.; Portalone, G.; Righini, G. *Inorg. Chem.* **2003**, *42*, 6345.
(29) (a) Bonavia, G.; Haushalter, R. C.; O'Connor, C. J.; Zubieta, J. *Inorg. Chem.* **1996**, *35*, 5603. (b) Calin, N.; Sevov, S. C. *Inorg. Chem.* **2003**, *42*, 7304. (c) Zheng, L.-M.; Yin, P.; Xin, X.-Q. *Inorg. Chem.* **1999**, *38*, 4618.
(30) Serre, C.; Ferey, G. *Inorg. Chem.* **1999**, *38*, 5370.
(31) Serre, C.; Ferey, G. *Inorg. Chem.* **2001**, *40*, 5350.
(32) Chakraborty, D.; Chandrasekhar, V.; Bhattacharjee, M.; Kra1tzner, R.; Roesky, H. W.; Noltemeyer, M.; Schmidt, H.-G. *Inorg. Chem.* **2000**, *39*, 23.
(33) Jaffrès, P.-A.; Caignaert, V.; Villemin, D. *Chem. Commun* **1999**, 1997.
(34) Hix, G. B.; Kariuki, B. M.; Kitchin, S.; Tremayne, M. *Inorg. Chem.* **2001**, *40*, 1477.
(35) Zhang, X.-M. *Coord. Chem. Rev.* **2005**, *249*, 1201.
(36) Zhang, X.-M. *Eur. J. Inorg. Chem.* **2004**, 544.
(37) Zhang, X.-M.; Fang, R.-Q.; Wu, H.-S. *Cryst. Growth Des.* **2005**, *5*, 1335.
(38) Rosi, N. L.; Kim, J.; Eddaoudi, M.; Chen, B.; O'Keeffe, M.; Yaghi, O. M. *J. Am. Chem. Soc.* **2005**, *127*, 1504.

Table 1. Crystallographic Data for Compound **1**

param	$C_{10}H_{26}N_2O_{15.5}P_2V_2$	$C_8H_{22}N_2O_{15.5}P_2V_2$
fw	586.15	558.09
cryst system	orthorhombic	orthorhombic
space group	Pnna	Pnna
a (Å)	7.0479(10)	7.0465(9)
b (Å)	15.307(2)	15.646(2)
c (Å)	17.537(3)	17.396(2)
V (Å^3)	1891.9(5)	1917.8(4)
Z	4	4
ρ_{calc} (g cm^{-3})	2.058	1.933
μ (mm^{-1})	1.246	1.224
F(000)	1200	1136
size (mm)	0.27 × 0.13 × 0.08	0.23 × 0.08 × 0.05
reflcns	8086/1852	7528/1485
T_{max}/T_{min}	0.9069 and 0.7296	0.9413 and 0.7660
data/params	1852/3/154	1485/46/138
S	1.100	0.978
R_1[a]	0.0549	0.0799
wR_2[b]	0.1333	0.2288
$\Delta\rho_{max}/\Delta\rho_{min}$ (e Å^{-3})	0.537, −0.962	2.151, −0.678

[a] $R_1 = \Sigma||F_o| - |F_c||/\Sigma|F_o|$; $wR_2 = [\Sigma w(F_o^2 - F_c^2)^2/\Sigma w(F_o^2)^2]^{1/2}$.

of the solution after reaction is 2. Phase purity was confirmed by comparison of measured and simulated XRPD patterns. Anal. Calcd for **1**, $C_{10}H_{26}N_2O_{15.5}P_2V_2$: C, 20.49; H, 4.47; N, 4.78. Found: C, 20.42; H, 4.53; N, 4.70.

H_2(PIP)[$V^{IV}O(H_2O)V^{III}(OH)(O_3PCH_2CO_2)_2$]·2.5$H_2O$ (2). A solution of $VOSO_4$ (0.97 g, 0.6 mmol), triethyl phosphonoacetate (0.124 g, 0.54 mmol), piperazine (PIP) (0.115 g, 0.6 mmol), and H_2O (7 mL) in the molar ratio of 1:0.9:1:650 was stirred, to which was added two drops of hydrofluoric acid (35%) to pH ≈ 5. The resulting solution was transferred into 15 mL Teflon-lined stainless steel reactor, which was heated at 170 °C for 200 h. After cooling of the sample to room temperature, dark green crystals of **2** (40%) were recovered. The measured pH value of the solution after reaction is 2. Anal. Calcd for **2**, $C_8H_{22}N_2O_{15.5}P_2V_2$: C, 17.22; H, 3.97; N, 5.02. Found: C, 17.18; H, 4.02; N, 4.96.

X-ray Crystallographic Study. Data were collected at 298 K on a Bruker Apex diffractometer (Mo Kα, λ = 0.710 73 Å). Lorentz−polarization and absorption corrections were applied. The structures were solved with direct methods and refined with the full-matrix least-squares technique (SHELX-97).[39] Analytical expressions of neutral-atom scattering factors were employed, and anomalous dispersion corrections were incorporated. All nonhydrogen atoms were refined anistropically. Hydrogen atoms of organic ligands were geometrically placed and refined with isotropic temperature factors. Hydrogen atoms of water molecules were located from difference Fourier map and refined with fixed temperature factors. The nitrogen atoms of piperazinium cation in **2** were disordered. The difference Fourier map corresponds to two solvent water molecules/formula in **1** and **2**, but EA and TGA revealed an additional half-water molecule. The crystallographic data for **1** and **2** are listed in Table 1; selected bond lengths and bond angles for **1** are given in Table 2.

Results and Discussion

Syntheses and IR Spectra. The synthesis route for **1** and **2** comprises the hydrothermal in situ reaction of trialkyl phosphonoacetate and V(IV) source, which is different from traditional routes for metal phosphonates. This route not only eliminates the need to synthesize the corresponding phosphonocarboxylic acid but also tends to afford large single crystals suitable for X-ray crystallography due to slow formation ligand and crystallization.[33−37] Another advantage is that the hydrolysis rate of trialkyl phosphonoacetate can be tuned by adjusting the pH and reaction temperature.

Table 2. Bond Lengths (Å) and Angles (deg) for **1**[a]

V(1)−O(1)	1.601(4)	V(2)−O(4)	1.985(2)
V(1)−O(2a)	1.992(3)	V(2)−O(4b)	1.985(2)
V(1)−O(2)	1.992(3)	P(1)−O(2)	1.520(3)
V(1)−O(6)	2.019(3)	P(1)−O(4)	1.523(3)
V(1)−O(6a)	2.019(3)	P(1)−O(3)	1.529(3)
V(1)−O(1W)	2.307(5)	P(1)−C(2)	1.805(4)
V(2)−O(7b)	1.9161(14)	O(5)−C(1)	1.220(5)
V(2)−O(7)	1.9161(14)	O(6)−C(1)	1.299(5)
V(2)−O(3c)	1.974(3)	C(1)−C(2)	1.503(6)
V(2)−O(3d)	1.974(3)		
O(1)−V(1)−O(2a)	99.06(8)	O(3c)−V(2)−O(4)	89.29(11)
O(1)−V(1)−O(2)	99.06(9)	O(3d)−V(2)−O(4)	90.71(11)
O(2a)−V(1)−O(2)	161.89(17)	O(7b)−V(2)−O(4b)	90.30(11)
O(1)−V(1)−O(6)	101.62(9)	O(7)−V(2)−O(4b)	89.70(11)
O(2a)−V(1)−O(6)	86.06(11)	O(3c)−V(2)−O(4b)	90.71(11)
O(2)−V(1)−O(6)	90.30(11)	O(3d)−V(2)−O(4b)	89.29(11)
O(1)−V(1)−O(6a)	101.62(9)	O(4)−V(2)−O(4b)	180.0
O(2a)−V(1)−O(6a)	90.30(11)	O(2)−P(1)−O(4)	111.85(15)
O(2)−V(1)−O(6a)	86.06(11)	O(2)−P(1)−O(3)	110.37(15)
O(6)−V(1)−O(6a)	156.76(19)	O(4)−P(1)−O(3)	112.28(14)
O(1)−V(1)−O(1W)	180.000(1)	O(2)−P(1)−C(2)	107.85(17)
O(2a)−V(1)−O(1W)	80.94(8)	O(4)−P(1)−C(2)	106.42(17)
O(2)−V(1)−O(1W)	80.94(8)	O(3)−P(1)−C(2)	107.80(18)
O(6)−V(1)−O(1W)	78.38(9)	P(1)−O(2)−V(1)	128.53(17)
O(6a)−V(1)−O(1W)	78.38(9)	P(1)−O(3)−V(2d)	132.38(15)
O(7b)−V(2)−O(7)	180.00(19)	P(1)−O(4)−V(2)	135.51(16)
O(7b)−V(2)−O(3c)	88.79(9)	C(1)−O(6)−V(1)	130.4(3)
O(7)−V(2)−O(3c)	91.21(9)	V(2)−O(7)−V(2d)	133.72(19)
O(7b)−V(2)−O(3d)	91.21(9)	O(5)−C(1)−O(6)	121.6(4)
O(7)−V(2)−O(3d)	88.79(9)	O(5)−C(1)−C(2)	121.1(4)
O(3c)−V(2)−O(3d)	180.0	O(6)−C(1)−C(2)	117.2(4)
O(7b)−V(2)−O(4)	89.70(11)	C(1)−C(2)−P(1)	115.7(3)
O(7)−V(2)−O(4)	90.30(11)		

[a] Symmetry codes: (a) $x, -y + 1/2, -z + 1/2$; (b) $-x, -y, -z + 1$; (c) $x - 1/2, y, -z + 1$; (d) $-x + 1/2, -y, z$.

The IR spectra of **1** and **2** (Figure S1, Supporting Information) show broad bands around 3400 cm^{-1}, consistent with the presence of hydrogen-bonded crystal lattice water molecules and diprotonated H_2(DABCO)/H_2(PIP) cations. The coordination of the carboxylates is seen from strong bands from the asymmetric and symmetric stretchings at 1627 and 1388 cm^{-1} in **1** and at 1602 and 1405 cm^{-1} in **2**. According to Nakamoto's studies, the $\Delta\nu$ value, a difference between asymmetric and symmetric bands, is useful to indicate the coordination modes of carboxylate group.[40] The $\Delta\nu$ values of 239 cm^{-1} in **1** and 197 cm^{-1} in **2** indicate unidentate mode of carboxylate, consistent with X-ray crystallography.[40] The set of intense bands at in the range of 900−1100 cm^{-1} in **1** is due to the stretching vibrations of the tetrahedral CPO_3 group. The stretching vibration of vanadyl V═O is indicated by strong bands at 945 cm^{-1} in **1** and 951 cm^{-1} in **2**.

Description of Structure. X-ray single-crystal diffraction reveals that **1** and **2** crystallize in orthorhombic space group *Pnna* and the asymmetric unit consists of two crystallo-

(39) Sheldrick, G. M. *SHELX-97, Program for X-ray Crystal Structure Solution and Refinement*; Göttingen University: Göttingen, Germany, 1997.

(40) Nakamoto, K. *Infrared and Raman Spectra of Inorganic and Coordination Compounds*; John Wiley & Sons: New York, 1986.

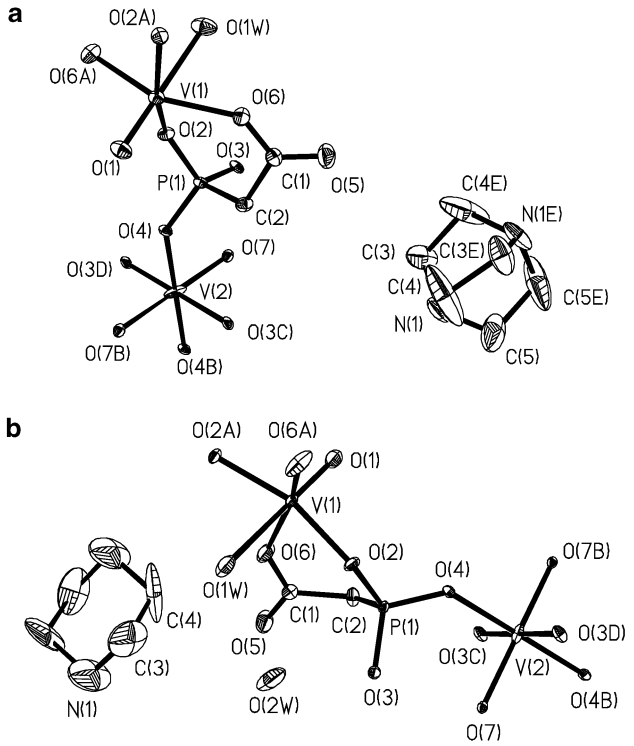

Figure 1. View of the coordination environments of vanadium sites in **1** (a) and **2** (b) with 35% thermal ellipsoid probability.

graphically independent vanadium sites, one phosphonoacetate (ppat), one vanadyl oxygen, one hydroxide, one coordinated water molecule, a half doubly protonated H_2(DABCO)/H_2(PIP), and some solvent water molecules as shown in Figure 1. For convenience, only **1** is described herein since **2** is isostructural with it. The V(1), V(2), O(1), and O(1w) sites occupy special positions with site occupancy of 0.5. The V(1) site shows a distorted octahedral geometry, being coordinated by two carboxylate oxygen atoms and two phosphonate oxygen atoms from two ppat groups in the equatorial plane [V(1)−O, 1.992(3) and 2.019(3) Å], one vanadyl oxygen [V(1)−O(1), 1.601(4) Å], and one water molecule [V(1)−O(1W), 2.307(5) Å] at axial positions. The *cis*-O−V(1)−O bond angles are in the range of 78.38(9)−101.62(9)° while the *trans*-O−V(1)−O bond angles are 156.76(19)−180.00(1)°. The V(2) site is on an inversion center and features regular octahedral geometry, ligated by four phosphonate oxygen atoms from four ppat groups and two hydroxide ions. The V(2)−O bond lengths are in the range 1.9161(14)−1.985(2) Å. The *cis*-O−V(2)−O bond angles are in the range 88.79(9)−91.21(9)° while the three *trans*-O−V(2)−O bond angles are 180.0°. The ppat group in a μ_3-mode is coordinated to two V(2) sites and one V(1) site via four oxygen atoms. The P(1) site shows a tetrahedral geometry, ligated by three oxygen atoms and one carbon atom. The P(1)−C(2) distance is 1.805(4) Å while the P(1)−O distances are in the range 1.520(3)−1.529(3) Å. The O−P(1)−O bond angles are in the range 110.37(15)−112.28(14)° while the O−P(1)−C bond angles are 106.42(17)−107.85(17)°.

Bond valence sum calculation by the curve of Brown and Altermatt showed that V(1) and V(2) sites have valence states

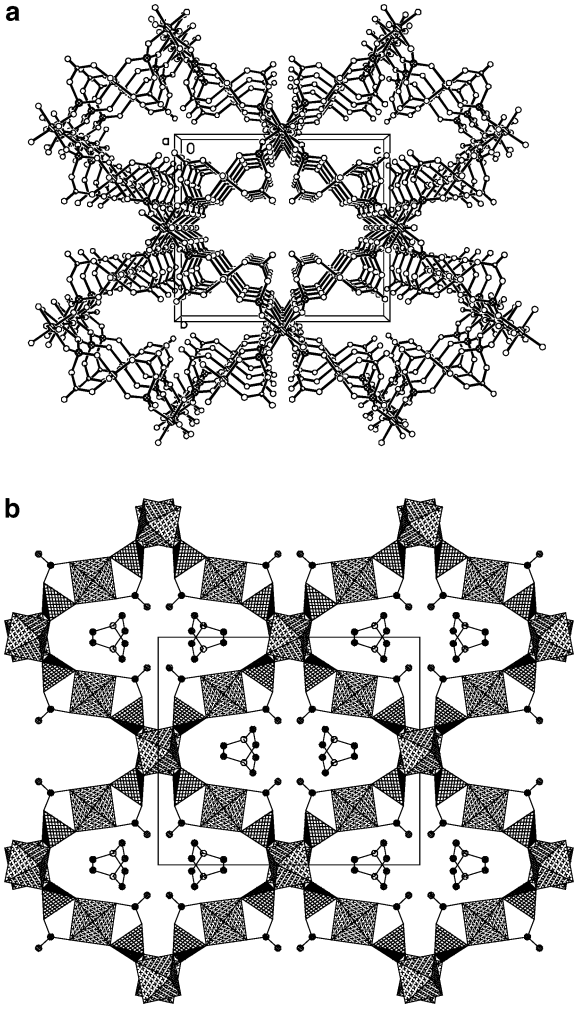

Figure 2. View of the 3-D open framework of **1** showing 1-D channels along the *a*-axis.

of 4.085 and 3.37, respectively.[41] In addition, Schindler proposed that the average equatorial bond lengths in VO_n polyhedra can be used to calculate valence state of vanadium sites.[42] For a tetravalent $V^{IV}O_6$ octahedron with one vanadyl bond, the average equatorial V−O bond length is typically of 2.00 Å.[42] For the $V(1)O_6$ octahedron with one vanadyl bond, the calculated average equatorial V−O bond length is 2.004 Å, further indicating that the V(1) site is tetravalent. No vanadyl bond and V(2)−O bond lengths of 1.88−2.18 Å (minimal and maximal bond length limits for $V^{III}O_6$ octahedron) suggest that the V(2) site is trivalent.[42] As indicated above, tetravalent and trivalent vanadium sites in **1** exhibit very different coordination geometries, and thus, **1** belongs to class I of the Robin and Day classification of mixed-valence compounds.

Compound **1** has a three-dimensional (3-D) framework featuring 16-ring ellipsoid channels with **sra** topology (Figure 2 and Scheme 1).[38] The V(2) atoms are bridged by the hydroxides to form a vanadium−oxygen chain with V(2)−O−V(2) angle 133° and V(2)−V(2) distance 3.526 Å. The adjacent vanadium−oxygen chains are linked by "metallo-

(41) Brown, I. D.; Altermatt, D. *Acta Crystallogr., Sect.* B **1985**, *41*, 244.
(42) Schindler, M.; Hawthorne, F. C.; Baur, W. H. *Chem. Mater.* **2000**, *12*, 1248.

Scheme 1 View of **Sra** Topology in **1** and **2**[a]

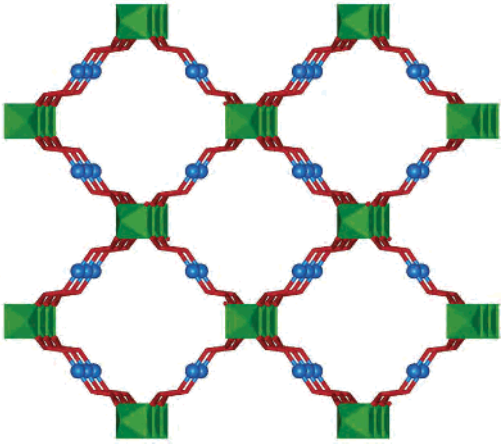

[a] The V(III) and V(IV) sites are shown as green octahedra and blue balls, respectively.

ligand" $[VO(H_2O)(ppat)_2]^{4-}$ to finish a 3D open framework featuring 16-membered ellipsoid channels along the *a*-axis. The effective length and width of the ellipsoid channel are ca. 14 and 5 Å. Calculation by PLATON[43] reveals that the volume of channels/unit cell is 789 Å^3, namely 41.7% of the total volume, which are filled with doubly protonated H_2(DABCO) cations and water molecules. There are strong hydrogen-bonding interactions among H_2(DABCO), water, and the inorganic framework. According to the classification approach in metal−organic frameworks constructed from rod-shaped secondary building units, the SBU in **1** consists of infinite $(-O-V-)_\infty$ rods with phosphonate O atoms completing octahedral coordination around V(2) to result in an infinite rod of VO_6 octahedra sharing opposite corners. Joining the $(-O-V-)_\infty$ rods through the −P−C−O−V(1)−O−C−P− links results in a 3-D net of the **sra** topology.[38]

Magnetic Properties. Magnetic properties of **1** and **2** is similar, and only those of **1** are described herein. The temperature dependence of the magnetic susceptibilities for **1** in the temperature range 2−320 K under a 1 kOe applied field was studied with in a Quantum Design SQUID MPMS XL-7. The $\chi_m T$ value at 320 K is 1.105 cm^3 K mol^{-1} and very slowly decreases to 1.094 cm^3 K mol^{-1} at 60 K (Figure 3). Upon further cooling, the $\chi_m T$ value rapidly increases to a value of 1.81 at 2 K. The corresponding effective magnetic moment (μ_{eff}) **1** increases from 2.97 μ_B at 320 K to 3.80 μ_B at 2 K. The magnetic data in the temperature range of 2−320 K follow the Curie−Weiss law with Curie constant C = 1.074 cm^3 K mol^{-1} and Weiss constant $\Theta = -1.34$ K. Assuming that V(IV) has a typical g value 1.96, the fit of the Curie constant 1.074 gives rise to the average g value of 1.69 for V(III), a value lower that typical g value of 1.79 for a V(III) ion.[44] The $M-H$ curve shows that the maximum magnetization is 2.38 $N\beta$ at 70 KOe, which is close to the saturation value 2.67 for one V(III) ($g = 1.69$) and one V(IV) ($g = 1.96$). No magnetic hysteresis and frequency dependence was observed. The convergence of ZFC and FC curves indicates that no magnetic order occurs at low temperature. Although the shape of $\chi_m T$ versus T curve resembles ferrimagnetic behavior, the $M-H$ curve in combination with the absence of magnetic hysteresis or frequency dependence indicates that **1** shows paramagnetic behavior. The increase of $\chi_m T$ values at low temperature possibly results from a little paramagnetic impurity.

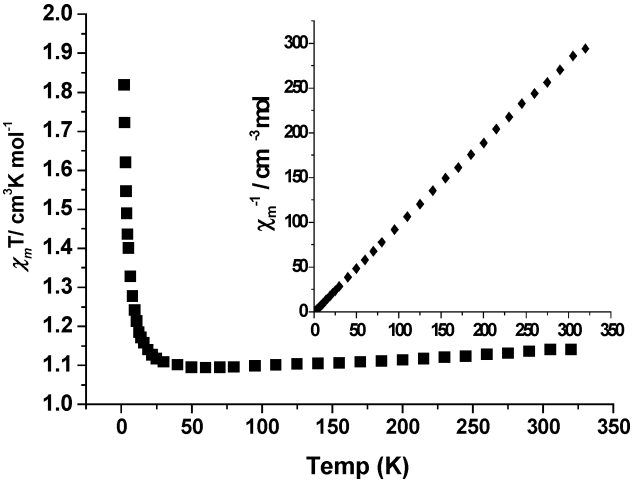

Figure 3. $\chi_m T$ versus T curve for **1** in the temperature range 2−320 K measured at an applied field of 1 KOe. Inset: χ_m^{-1} versus T curve.

From magnetic point of view, **1** can be seen as a 3D lattice formed by crossing linkages of $[-V(III)-O]_\infty$ and $[-V(III)-O-P-O-V(IV)-O-P-O]_\infty$, two types of chains (Scheme 1). There are two possible superexchange routes [V(III)−V(III) via oxo bridge and V(III)−V(IV) via phosphonate bridge]. The octahedral V(III) ions are bridged by hydroxides to form a $[V(III)-O]_\infty$ chain similar to that observed in MIL-47as.[45] According to the Goodenough rules,[46] V(III)−V(III) interactions are predicted to be ferromagnetic if the superexchange angle is close to 180°, with vanadium in an octahedral coordination site, but the sign of the exchange integral J can be inverted when the V(III)−O−V(III) angle decreases below the so-called "blank angle". The V(III)−O−V(III) superexchange angle in MIL-47as is 124°, an angle thought to be lower than the "blank angle" due to the observation of intrachain antiferromagnetic interactions. In contrast, the V(III)−O−V(III) angle in **1** is 133° that possibly is close to the "blank angle". As for the exchange interactions between V(III) and V(IV) ions, the large separation of 6.08 Å between adjacent V(III) and V(IV) ions and poor electron transmitting nature of the O−P−O bridges eliminate or reduce the probability of a double-exchange mechanism, resulting into little or no magnetic exchange interactions between V(III) and V(IV) ions.[47]

Thermal Behavior. Compounds **1** and **2** show similar thermal behavior as shown in Figure 4. An initial mass loss

(43) Spek, A. L. *PLATON, A Multipurpose Crystallographic Tool*; Untrecht University: Utrecht, The Netherlands, 1999.
(44) Millet, P.; Mila, F.; Zhang, F. C.; Mambrini, M.; Van Oosten, A. B.; Pashchenko, V. A.; Sulpice, A.; Stepanov, A. *Phys. Rev. Lett.* **1999**, *83*, 4176.
(45) Barthelet, K.; Marrot, J.; Riou, D.; Ferey, G. *Angew. Chem., Int. Ed.* **2002**, *41*, 281.
(46) Goodenough, J. B. In *Magnetism and the Chemical Bond*; Interscience: New York, 1963.
(47) Borras-Almenar, J. J.; Clemente-Juan, J. M.; Coronado, E.; Palii, A.; Tsukerblat, B. S. In *Magnetism: Molecules to Materials*; Miller, J. S., Drillon, M.; Eds.; Wiley-VCH: Weiheim, Germany, 2002; Vol. 1, pp 155−210.

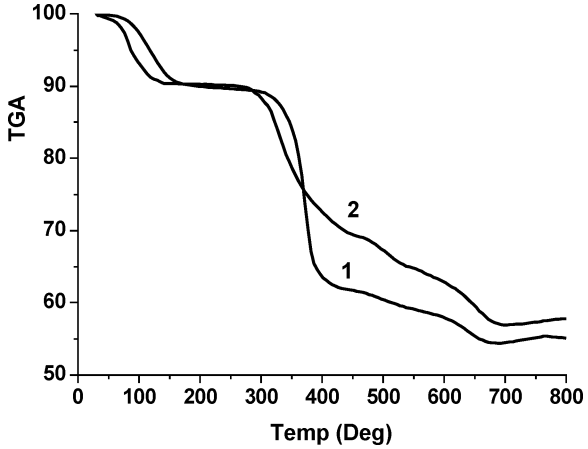

Figure 4. TGA curves of **1** and **2** in air with the heating rate of 10 °C/min.

of 10.5% (calcd 10.75%) for **1** and 11.2% (calcd 11.29%) for **2** below 295 °C is attributed to loss of the trapped water molecules/formula. The following total mass loss of 35.1% for **1** and 31.7% for **2** in the temperature range 340−690 °C is thought to be due to removal of H_2(DABCO)/H_2(PIP) and decomposition of ppat into phosphate. The residue percentage of 54.4% for **1** and 56.9% for **2** at 690 °C indicates a new phase with empirical formula $V_2P_2O_{10}H_2$. Upon further heating, the slight increase of weight corresponds to uptake of oxygen accompanied by valence state change of vanadium ions.

Conclusion

A vanadium phosphonoacetate characterized by the mixed-valence V(III,IV) and 16-ring channels has been synthesized by hydrothermal hydrolysis of trialkyl phosphonoacetate route. The hydrolysis of trialkyl phosphonoacetate during the course of the hydrothermal synthetic procedure not only removes the need to synthesize the corresponding phosphonocarboxylic acid but also tends to provide large single crystals suitable for X-ray crystallography. In contrast to other microporous metal phosphonocarboxylates, compound **1** contains infinite $(-O-V-)_\infty$ chains that are cross-linked by the "metalloligand" $[VO(H_2O)(O_3PCH_2CO_2)_2]^{4-}$ into a 3-D net of the **sra** topology.[38] The presence of mixed-valence V(III)/V(IV) sites and one-dimensional channels in **1** may indicate potential redox catalysis and zeolite-like behavior.

Acknowledgment. This work was financially supported by the NSFC (Grant 20401011), A Foundation for the Author of a National Excellent Doctoral Dissertation of P. R. China (Grant 200422), A Program for New Century Excellent Talents in University (NCET), and the Youth Academic Leader of Shanxi and Returned Overseas Students of Shanxi.

Supporting Information Available: Crystal structure data for **1** in CIF format, XRPD, an *M*−*H* curve, and IR spectra. This material is available free of charge via the Internet at http://pubs.acs.org.

IC060771P